

05,11

Spiral magnetic order and metal-insulator transition in the Hubbard model on a triangular lattice

© V.F. Gilmutdinov, M.A. Timirgazin, A.K. Arzhnikov

Udmurt Federal Research Center, Ural Branch Russian Academy of Sciences, Izhevsk, Russia

E-mail: vital@udman.ru

Received August 18, 2021

Revised August 18, 2021

Accepted September 4, 2021

The magnetic phase diagrams of the two-dimensional Hubbard model for isotropic and anisotropic triangular lattices are constructed within the Hartree–Fock and slave boson approximations. The triangular lattice specific non-collinear and spiral magnetic states, as well as phase separation between them, are shown to be realized in a wide range of model parameters along with collinear magnetic states (stripe antiferromagnetic and ferromagnetic). Phase transitions of the first and second order are found, and the boundaries of the phase separation regions are determined. A comparison of the two approximations, Hartree–Fock and slave boson, shows that electronic correlations suppress magnetic states, the region of paramagnetism being expand, for values $U/t \gtrsim 5$. At the same time, when the Fermi level is near the van Hove singularity, electron correlations do not change the diagrams qualitatively, which is consistent with the previously obtained result for square and cubic lattices. The results are compared with the data available in the literature for other methods and approaches.

Keywords: Hubbard model, phase separation, spiral magnetic order, triangular lattice, metal-insulator transition

DOI: 10.21883/PSS.2022.01.52492.191

1. Introduction

Of particular interest in the study of magnetic properties of strongly correlated electron systems are compounds with frustrated magnetic states. They include, for instance, organic superconductors (based on BEDT-TTF molecules), sodium cobaltites Na_2CoO_x etc. The quasi-two-dimensional conductivity is caused due to each dimer of BEDT-TTF molecules have one localized electron and efficiently forms layers of triangular lattices, anions being located between them [1]. Due to geometric frustration, staggered (Neel) antiferromagnetic (AF) ordering can not emerge form in lattices of this type, but other magnetic structures, not typical for square- and cubic-lattice systems, stabilize. Anderson has shown in [2] that has showed that the ground state in a triangular lattice may be a quantum-mechanical superposition of singlet pairs that inhabit the lattice. This new state of matter called „spin liquid“ has unique properties, in particular, excited states can be spinons (magnetic objects having a zero electric charge).

The data of experimental studies [3,4] shows the formation of both a collinear AF and (incommensurate) noncollinear magnetic configurations in triangular-lattice systems. Theoretical calculations within the framework of the Hubbard model, traditionally used to describe the magnetism and superconductivity of strongly correlated electron systems, also predict the formation of various magnetic states.

Magnetic phase diagrams (MPD) of the Hubbard model for an anisotropic triangular lattice in the unrestricted

Hartree–Fock method (HF) (both charge and spin fluctuations with a certain weight coefficient are taken into account) were obtained in the paper [5]. Collinear ferromagnetic (FM) and stripe AF orderings, as well as complanar and noncomplanar spiral phases were considered. The stabilization of noncollinear magnetic states in a wide region of model parameters, as well as magnetic phase separation (PS) between them was shown.

Electron correlations were accounted using the slave boson approximation (SB) of Kotliar and Ruckenstein for the Hubbard model in the papers [6] and [7]. The authors of the article [6] constructed of the Hubbard model with account of AF, paramagnetic (PM) states and the linearly polarized spin density wave. A first-order phase transition between the AF and PM states was found. MPDs of the Hubbard model are presented in [7], charge and sping orderings and electron transfer within the first three coordination spheres being taken into account.. First- and second-order phase transitions between different magnetic phases were found. Both above-mentioned studies are presented in a limited range of model parameters and ignore all possible spiral magnetic states with a variable wave vector.

A separate line of research is related to study of the metal–insulator transition (MIT), taking place at half-filling when increasing the interaction parameter. Thereat, special attention is paid to searching a region of stable non-magnetic insulator, showing the possibility of spin liquid formation [8]. MIT was previously considered within the framework of

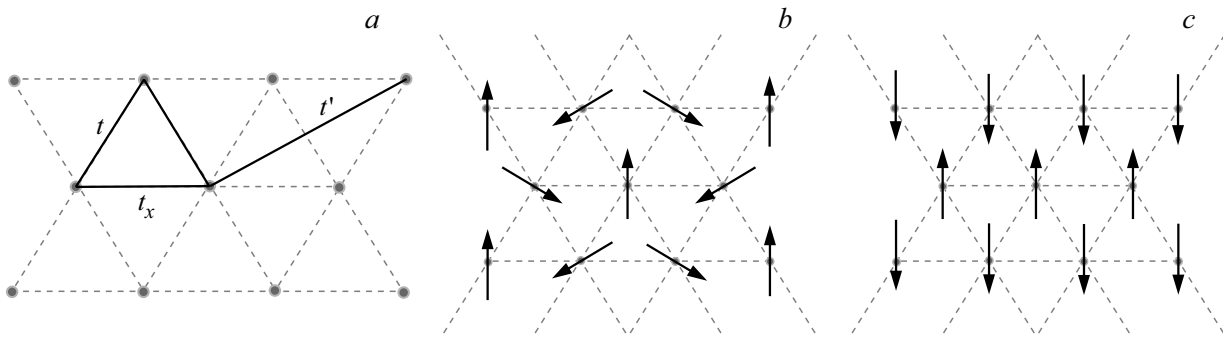


Figure 1. a) Integrals of carryover in a triangular-lattice system, b) 120° -structure, c) stripe ordering.

variational cluster approximation (VCA) [9,10], unrestricted Hartree–Fock method (UHF) [5], renormalization group functional (fRG) [11–13], cellular dynamical mean-field theory (DMFT) [14], Monte–Carlo method [15], combination of UHF and variational Monte–Carlo [16]. Within the framework of the SB approximation, it was shown that in the systems with triangular lattice, MIT occurs at a finite value of U , in contrast to the case of a square lattice, where perfect nesting of the Fermi surface leads to MIT and AF ordering at arbitrarily small values of the Hubbard parameter U [17]. Depending on chosen approach and model parameters, both the magnetic MIT in the presence of AF and various noncollinear magnetic states and the Mott paramagnetic MIT have been obtained. The spin liquid state was found to be stable for the values of the electron transfer integral corresponding to BEDT-TTF compounds in the weak correlation mode $4 \lesssim U/t \lesssim 10$ [10].

Despite the fact that significant attention is being paid for a long time to the study of magnetic properties of quasi-two-dimensional triangular-lattice electron systems, the data presented thus far in the literature is incomplete. In particular, the range of used model parameters or considered magnetic phases is limited [6], or consideration of spiral states with a random wave vector of the magnetic spiral is ignored [5], etc. Up to now, no studies with successive consideration of random wave vectors of a magnetic spiral with simultaneous comparison of results of the HF and SB methods have been carried out. Such a comparison would make it possible to determine the role of electron correlations in the formation of magnetic states in triangular-lattice electron systems. At the same time, this manner was successfully used to describe magnetic properties of cubic- and square-lattice systems. The conditions of stabilization of spiral magnetic states were previously studied in the SB approximation for a Hubbard model in the paper [18], where MPDs were obtained taking into account the possibility of PS. This approach has been also successfully used to describe magnetic states on a frustrated face-centered cubic lattice [19].

2. Formalism

We consider the ground state of a single-band Hubbard model on a triangular lattice. The model Hamiltonian in the site representation has the form

$$H = \sum_{j,j',\sigma} t_{j,j'} c_{j,\sigma}^\dagger c_{j',\sigma} - \mu \sum_{j,\sigma} c_{j,\sigma}^\dagger c_{j,\sigma} + U \sum_j n_{j,\uparrow} n_{j,\downarrow}, \quad (1)$$

where $t_{j,j'}$ is the integral of electron transfer from site j to site j' , $c_{j,\sigma}^\dagger$ ($c_{j,\sigma}$) is the operation of creation (annihilation) of an electron having the spin $\sigma = (\uparrow, \downarrow)$ on site j , U is the on-site value of electron's Coulomb interaction, $n_{j,\sigma} = c_{j,\sigma}^\dagger c_{j,\sigma}$ is the operator of density of electrons having the spin σ on site j , μ is the chemical potential. We take into account the electron transfer within the first and second coordination spheres with integrals $-t$ and t' , respectively, thereat, anisotropy was introduced in the assigned direction x ($t_x \neq t$) (see Fig. 1, a). Therefore, the free electrons' energy spectrum is as follows

$$\varepsilon_{\mathbf{k}} = -2t_x \cos k_x - 4t \cos \frac{k_x}{2} \cos \frac{k_y \sqrt{3}}{2} + 2t' \left(\cos k_y \sqrt{3} + 2 \cos \frac{3k_x}{2} \cos \frac{k_y \sqrt{3}}{2} \right). \quad (2)$$

We take into consideration the whole variety of spiral magnetic states, thereat, the calculations show that the following magnetic order types are implemented in the ground state: 120° -structure (see Fig. 1, b) with $\mathbf{Q} = (0, 4\pi/3)$, collinear stripe ordering (see Fig. 1, c) with $\mathbf{Q} = (0, 2\pi/\sqrt{3})$, as well as spiral magnetic states with wave vectors $\mathbf{Q}: (0, Q), (Q, 0)$ and $(Q, 2\pi/\sqrt{3})$.

The magnetic state on the site j can be described by the following magnetic moment vector

$$\mathbf{m}_j = m(\cos \mathbf{Q}\mathbf{R}_j, \sin \mathbf{Q}\mathbf{R}_j), \quad (3)$$

where m is the magnetic moment amplitude, \mathbf{R}_j is the radius-vector of node j .

The operation of conversion of the SU(2)-rotation at the angle of \mathbf{QR}_j around axis z allows for treat the spiral magnetic states as the FM order.

$$\widehat{A}(\mathbf{R}_j) = e^{i(n\widehat{\sigma})\frac{\mathbf{QR}_j}{2}} = \sigma^0 \cos \frac{\mathbf{QR}_j}{2} + i(n\widehat{\sigma}) \sin \frac{\mathbf{QR}_j}{2}, \quad (4)$$

where \mathbf{R}_j is the radius-vector of site j , \mathbf{Q} is the wave vector of magnetic spiral, \mathbf{n} is the unit vector, which direction corresponds to the orientation of magnetic moment m on the site, $\widehat{\sigma}^0$ is the unit matrix, $\widehat{\sigma} = (\widehat{\sigma}^x, \widehat{\sigma}^y, \widehat{\sigma}^z)$ are SU(2) rotation group generators (Pauli matrices).

2.1. Hartree–Fock method

After rotation and Fourier transformation in the HF approximation, the Hamiltonian operator (1) takes the form of

$$H^{\text{HFA}} = \sum_{\mathbf{k}, \sigma, \sigma'} t_{\mathbf{k}}^{\sigma, \sigma'} c_{\mathbf{k}, \sigma}^\dagger c_{\mathbf{k}, \sigma'} - \mu \sum_{\mathbf{k}, \sigma} c_{\mathbf{k}, \sigma}^\dagger c_{\mathbf{k}, \sigma} + \frac{NU}{4} (m^2 - n^2) + \frac{Un}{2} \sum_{\mathbf{k}, \sigma} c_{\mathbf{k}, \sigma}^\dagger c_{\mathbf{k}, \sigma} - \frac{Um}{2} \sum_{\mathbf{k}, \sigma} \sigma c_{\mathbf{k}, \sigma}^\dagger c_{\mathbf{k}, \sigma},$$

$$t_{\mathbf{k}}^{\sigma, \sigma'} = e_{\mathbf{k}}^s \delta_{\sigma, \sigma'} + e_{\mathbf{k}}^a \delta_{\sigma, \sigma'},$$

$$e_{\mathbf{k}}^s = \frac{\varepsilon_{\mathbf{k}+\frac{\mathbf{Q}}{2}}^0 + \varepsilon_{\mathbf{k}-\frac{\mathbf{Q}}{2}}^0}{2},$$

$$e_{\mathbf{k}}^a = \frac{\varepsilon_{\mathbf{k}+\frac{\mathbf{Q}}{2}}^0 - \varepsilon_{\mathbf{k}-\frac{\mathbf{Q}}{2}}^0}{2}.$$

Here, N is the total number of particles in the system, $n = \langle \sum_{\mathbf{k}, \sigma} c_{\mathbf{k}, \sigma}^\dagger c_{\mathbf{k}, \sigma} \rangle$ and $m = \langle \sum_{\mathbf{k}, \sigma} \sigma c_{\mathbf{k}, \sigma}^\dagger c_{\mathbf{k}, \sigma} \rangle$ are average values of electron density and magnetic moment, respectively. System state is determined by minimization of thermodynamic potential $\Omega_{\text{HFA}} = \langle H^{\text{HFA}} \rangle$ for each configuration of system parameters $\Omega_{\text{HFA}} = \text{argmin} \Omega_{\text{HFA}}(\mu, \mathbf{Q}, U)$ ($\langle \dots \rangle$ means quantum-mechanical averaging by the ground state of the Hamiltonian operator).

2.2. Method of slave bosons

We use the SB method in a saddle point approximation in the Kotliar and Ruckenstein treatment [20], the formalism is being described in detailed enough, e.g. in the paper [18]. Upon conversion of the rotation (4), SB operators e_j , $p_{j, \sigma}$ and d_j are introduced; they correspond to an empty site, a site occupied by one and two electrons j , and limitations that exclude non-physical states are imposed:

$$e_j^\dagger e_j + \sum_{\sigma} p_{j, \sigma}^\dagger p_{j, \sigma} + d_j^\dagger d_j = 1, \quad (5)$$

$$p_{j, \sigma}^\dagger p_{j, \sigma} + d_j^\dagger d_j = c_{j, \sigma}^\dagger c_{j, \sigma}.$$

A substitution that ensures coherence of bosonic and fermionic fields is done in the Kotliar and Ruckenstein treatment: $c_{j, \sigma} \rightarrow z_{j, \sigma} f_{j, \sigma}$, where

$$z_{j, \sigma} = (1 - d_j^\dagger d_j - p_{j, \sigma}^\dagger p_{j, \sigma})^{-1/2} \times (e_j^\dagger p_{j, \sigma} + p_{j, \sigma'}^\dagger d_j) (1 - d_j^\dagger d_j - p_{j, \sigma'}^\dagger p_{j, \sigma'})^{-1/2}. \quad (6)$$

The term $e_j^\dagger p_{j, \sigma}$ corresponds to a transition from a singly occupied state into an empty state, while $p_{j, \sigma'}^\dagger d_j$ — to a transition from a twice occupied state to a single one. The Hamiltonian in the introduced parametrization takes a diagonal form in relation to boson operators

$$H^{\text{SBA}} = \sum_{j, j', \sigma, \sigma'} t_{j, j'}^{\sigma, \sigma'} c_{j, \sigma}^\dagger c_{j', \sigma'} z_{j, \sigma}^\dagger z_{j', \sigma'} + U \sum_j d_j^\dagger d_j. \quad (7)$$

In a static approximation, thermodynamic potential of a grand canonical ensemble of the system is as follows

$$\Omega_{\text{SBA}} = \eta (e^2 + p_\uparrow^2 + p_\downarrow^2 + d^2 - 1) + U d^2 - \sum_{\sigma} \lambda_{\sigma} (p_{\sigma}^2 + d^2) + \Omega_f. \quad (8)$$

Here, λ_{σ} and η are Lagrange multipliers, while Ω_f is the standard thermodynamic potential of a fermion system. Minimization of thermodynamic potential in relation to the wave vector \mathbf{Q} makes it possible to determine the system's ground magnetic state at the chosen parameters ($U/t, n$) and to construct MPD of the model.

3. Results

3.1. ($U/t, n$)-diagrams

The results are shown in Figs. 2 and 3, respectively. MPD show that both collinear (stripe, FM) and spiral (120° -structure, phases with a variable wave vector $(0, Q)$, $(Q, 0)$, and $(Q, 2\pi/\sqrt{3})$) magnetic states are implemented in the system. These diagrams were constructed without taking into account the anisotropy of the electron transfer integral and the electron transfer onto the next-nearest neighbor sites.

A PS between different states is implemented in a wide region of the diagram parameters. Chemical potential μ is used as a base variable to consider the possibility of PS, while number of electrons n is a parameter. The first-order phase transition, accompanied by PS, is characterized by a jump in the magnetic structure parameters \mathbf{Q} and m : from (\mathbf{Q}_1, m_1) to (\mathbf{Q}_2, m_2) . This transition in variables (U, μ) is also characterized by the jump $\Delta(n) = |n(\mu, \mathbf{Q}_1, m_1) - n(\mu, \mathbf{Q}_2, m_2)|$. If n lies between $n(\mu, \mathbf{Q}_1, m_1)$ and $n(\mu, \mathbf{Q}_2, m_2)$, the system simultaneously has two spatially separated phases with densities $n(\mu, \mathbf{Q}_1, m_1)$ and $n(\mu, \mathbf{Q}_2, m_2)$ that determine the left and right boundaries of the PS region on the MPD [21].

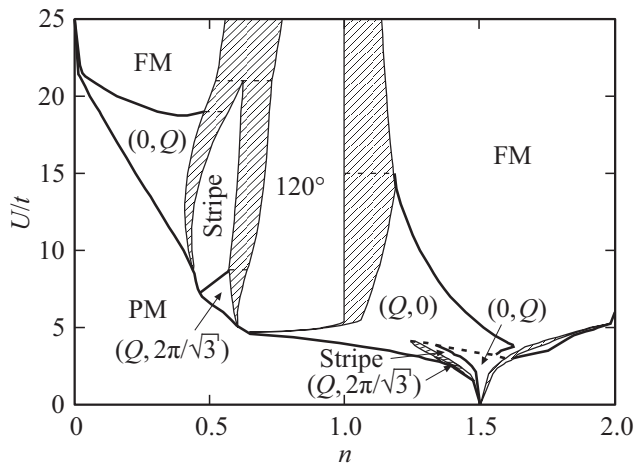


Figure 2. Magnetic phase diagram of the ground state of the Hubbard model for a triangular lattice constructed in the HF approximation. The thick lines denote the boundaries of the second-order phase transitions, the thin lines separate the regions of the homogenous phase and phase separation (shaded regions). The thin dashed horizontal lines separate the phase separation regions for different phase pairs. The thick dashed lines show the first-order phase transitions. The abbreviations „PM“, „FM“ and „Stripe“ designate the regions of the paramagnetic, ferromagnetic and stripe states, respectively. Regions of spiral spin ordering with a variable wave vector are designated with the projections of the magnetic spiral wave vector indicated in brackets.

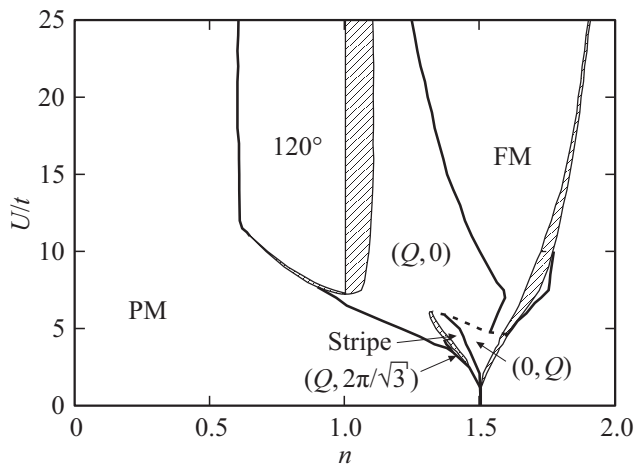


Figure 3. Magnetic phase diagram of the ground state of the Hubbard model for a triangular lattice plotted in the SB approximation. The designations are the same as in Fig. 2.

There are a few differences between the diagrams for the HF and SB methods. The use of the SB method causes a suppression of the magnetic order by strong electron correlations, and the region of ordered phases narrows towards the half-filling line. For $U/t > 5$ there is a significant decrease of the variety of spiral magnetic phases: only the state $(Q, 0)$ from the among them is implemented in the $n > 1$, while at $n < 1$ the consideration of strong electron correlations causes complete disappearance of the

stripe, spiral and FM states. At $U/t < 5$ the variety of spiral states remains, but the diagram appearance changes at the quantitative level: PM region extends significantly. Moreover, in the SB method for values $U/t > 5$: PS regions between paramagnetic and magnetic states appear (with the 120° -state in the region of hole doping and with FM — in the region of electron doping). For a diagram constructed in the HF approximation, all transitions to a PM state at the specified values of U/t are of the second-order and are not accompanied with phase separation.

As U/t increases, the region of the FM state in the $n > 1$, becomes larger. This with the Nagaoka theorem which point out that the ground state of the Hubbard model on a triangular lattice within $U \rightarrow \infty$ in case of one-electron doping (which is equivalent to hole doping at $t > 0$) is saturated FM [22,23]. A similar result has been obtained previously for another frustrated system — FCC lattice [19].

The investigation [5] deals with noncomplanar states, however, as distinct from our paper, it does not take into account the whole variety of spiral states. Moreover, in the investigation mentioned above the nature of phase transitions between magnetic states. The consideration of different sets of magnetically ordered phases and a difference in applied approaches lead to qualitative and quantitative differences. A stripe state in the hole-doped region of our diagram exists within $6 \lesssim U/t \lesssim 21$, while in the paper [5] it in the absence of anisotropy of the electron transfer integral and appears only with increase of the anisotropy value in the narrow region of the parameter $10 \lesssim U/t \lesssim 15$. The FM state on our diagrams undergoes a phase separation with the 120° -structure in the hole doping region at $U/t > 15$. In the study [5], phase separation in the same region with a conical spiral structure, followed by a FM phase. At the same time, in the interval of parameters $0.6 \lesssim n \lesssim 1$ and $5 \lesssim U/t \lesssim 15$ and $1.4 \lesssim n \lesssim 2.0$ and $5 \lesssim U/t \lesssim 15$ our results are in agreement with the results given in the paper [5].

3.2. Metal–insulator transition

Figures 4 and 5 show the MPDs in coordinates $(t'/t, U/t)$ at $n = 1$, constructed using the SB method, for two cases: 1) isotropic electron transfer t with account of jumps to the next-nearest neighbor sites t' and 2) with anisotropy of electron transfer $(t, t_x; \text{ see Fig. 1})$. The diagrams have regions of a metallic state with paramagnetic and spiral magnetic ordering, as well as an insulating state with stripe, spiral and 120° -structure ordering. Transitions between states with a permanent wave vector and transition from a metallic state to an insulating state are of first order. Second-order phase transitions happens from a stripe magnetic state to a spiral insulating state, as well as transitions from PM to a spiral metallic state. In addition, both diagrams (inserts) show the transitions from a PM-metallic state to a PM-insulating (PI). This is a second-order phase transition, for the isotropic case it occurs at $U/t > 16$, for an anisotropic state at $U/t > 13$. It can be

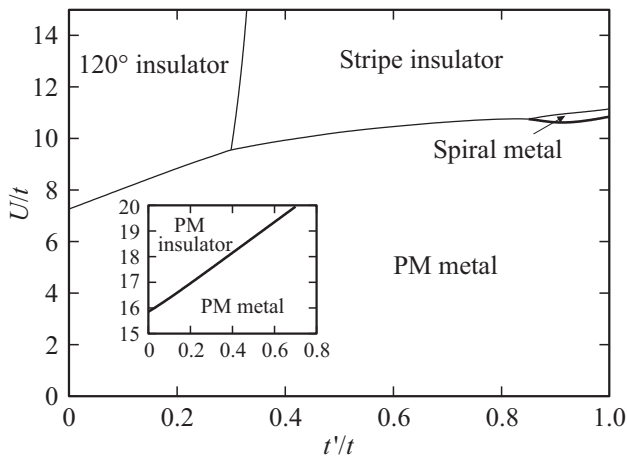


Figure 4. Phase diagram of the Hubbard model in the SB approximation for $n = 1$, taking into account the electron transfer to the first t and second t' coordination spheres. The heavy lines show second-order phase transitions, thin ones — first-order transitions. The region of „spiral metal“ corresponds to the wave vector $(Q, 2\pi/\sqrt{3})$. The insert shows an identical phase diagram plotted exclusive of magnetic states.

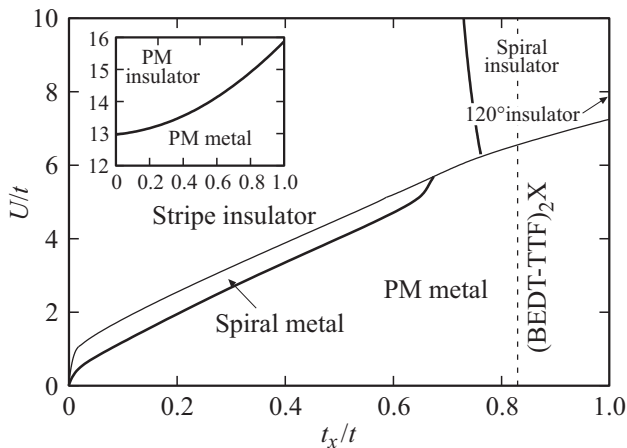


Figure 5. Phase diagram of the Hubbard model in the slave boson approximation in variables $(t_x/t, U/t)$ taking into account the anisotropy of the electron transition integral along the x axis. A vertical dashed line shows the value t_x/t , corresponding to BEDT-TTF organic superconductors. The other designations are the same as in Fig. 4. The insert shows an identical phase diagram plotted exclusive of magnetic states.

seen from the MPD that the magnetic states stabilize at such high values of U/t , thus, the PI state is not the ground state, which means that the spin liquid is not found in our approach.

MIT on a triangular lattice has been previously considered using the VCA method in the [9], which obtained a significantly lower critical value of the interaction parameter $U/t \sim 4$, so that the authors claimed the formation of a spin liquid state. A MPD of the Hubbard model in the coordinates $(U/t, t_x/t)$ was plotted in [10,11] at $n = 1$ within

the framework of the VCA method and the renormalization group method. There are obtained the state of a non-magnetic insulator in the region of parameters $5 \lesssim U/t \lesssim 9$ and $0.8 \lesssim n \lesssim 1$. The disadvantage of mentioned studies is the ignoring of the spin spiral state which is the ground state in our calculations.

Diagram 5 has a vertical dashed line at the value of $t_x/t = 0.83$, corresponding to organic superconductors based on BEDT-TTF [16]. Thus, we conclude that our research predicts a first-order transition from a paramagnetic metallic state to a magnetic insulating state with a spiral spin structure upon an increase in the parameter U/t for such the organic superconductors.

4. Conclusion

We have studied the conditions of formation of magnetic states on an isotropic and anisotropic triangular lattice in the Hubbard model. The HF and SB approximations were used. We have found that, along with collinear magnetic states (FM, stripe AF), spiral magnetic states with wave vectors $(0, Q)$, $(Q, 0)$ and $(Q, 2\pi/\sqrt{3})$ also emerges in triangular-lattice systems. Consideration of electron correlations causes an extension of the PM state region and reduces the variety of magnetic phases, which agrees with the previously obtained results for the square and cubic lattices [18]. The formation of a 120° - structure in the and the extension of the concentration region of PM existence upon a decrease in the parameter U/t is typical both for our research and for other authors' studies. A considerable difference of our approach is the accounting of the whole variety of spiral magnetic states, as well as phase separation regions that occupy the significant part of the diagrams. This results, in particular, in a wide region of magnetic states on metal–insulator transition diagrams, which displaces the magnetic insulator region.

Funding

The work has been performed under the state assignment of the Ministry of Science and Higher Education of the Russian Federation (topic No. 121030100005-1).

Conflict of interest

The authors declare that they have no conflict of interest.

References

- [1] Y. Shimizu, K. Miyagawa, K. Kanoda, M. Maesato, G. Saito. Phys. Rev. Lett. **91**, 10, 107001 (2003).
- [2] P.W. Anderson. Mater. Res. Bull. **8**, 2, 153 (1973).
- [3] P. Limelette, P. Wzietek, S. Florens, A. Georges, T.A. Costi, C. Pasquier, D. Jérôme, C. Mézière, P. Batail. Phys. Rev. Lett. **91**, 1, 016401 (2003).

- [4] H. Nakamura, T. Yamasaki, S. Giri, H. Imai, M. Shiga, K. Kojima, M. Nishi, K. Kakurai, N. Metoki. *J. Phys. Soc. Jpn* **69**, 9, 2763 (2000).
- [5] K. Pasrija, S. Kumar. *Phys. Rev. B* **93**, 19, 195110 (2016).
- [6] A. Feiguin, C. Gazza, A. Trumper, H. Ceatto. *J. Phys.: Condens. Matter* **9**, 4, L27 (1999).
- [7] K. Jiang, S. Zhou, Z. Wang. *Phys. Rev. B* **90**, 16, 165135 (2014).
- [8] T. Mizusaki, M. Imada. *Phys. Rev. B* **74**, 1, 014421 (2006).
- [9] K. Misumi, T. Kaneko, Y. Ohta. *Phys. Rev. B* **95**, 7, 075124 (2017).
- [10] M. Laubach, R. Thomale, C. Platt, W. Hanke, G. Li. *Phys. Rev. B* **91**, 24, 245125 (2015).
- [11] H. Morita, S. Watanabe, M. Imada. *J. Phys. Soc. Jpn* **71**, 9, 2109 (2002).
- [12] Z. Zhu, D.N. Sheng, A. Vishwanath. arXiv:2007.11963 (2020).
- [13] A. Szasz, J. Motruk. arXiv:2101.07454 (2021).
- [14] B. Kyung, A.-M.S. Tremblay. *Phys. Rev. Lett.* **97**, 4, 046402 (2006).
- [15] L. Tocchio, A. Montorsi, F. Becca. *Phys. Rev. B* **102**, 11, 115150 (2020).
- [16] L. Tocchio, H. Feldner, F. Becca, R. Valentí, C. Gros. *Phys. Rev. B* **87**, 3, 035143 (2012).
- [17] M. Capone, L. Capriotti, F. Becca, S. Caprara. *Phys. Rev. B* **63**, 8, 085104 (2000).
- [18] P.A. Igoshev, M.A. Timirgazin, V.F. Gilmutdinov, A.K. Arzhnikov, V.Y. Irkhin. *J. Phys.: Condens. Matter* **27**, 44, 446002 (2015).
- [19] M.A. Timirgazin, P.A. Igoshev, A.K. Arzhnikov, V.Y. Irkhin. *J. Phys.: Condens. Matter* **28**, 50, 505601 (2016).
- [20] G. Kotliar, A.E. Ruckenstein. *Phys. Rev. Lett.* **57**, 11, 1362 (1986).
- [21] P.A. Igoshev, M.A. Timirgazin, A.A. Katanin, A.K. Arzhnikov, V.Y. Irkhin. *Phys. Rev. B* **81**, 9, 094407 (2010).
- [22] Y. Nagaoka. *Phys. Rev.* **147**, 1, 392 (1966).
- [23] H. Tasaki. *Phys. Rev. B* **40**, 13, 9192 (1989).